Available online at www.sciencedirect.com
SCIENCE DIRECT®
Journal of Sound and Vibration 272 (2004) 267–286
JOURNAL OF SOUND AND VIBRATION
www.elsevier.com/locate/jsvi

The periodic impact responses and stability of a human body in a vehicle traveling on rough terrain

Ke Yu[a], Albert C.J. Luo[b,*]

[a] *Department of Mechanical Engineering, Washington University, Campus Box 1185, St. Louis, MO 63130-4899, USA*
[b] *Department of Mechanical and Industrial Engineering, Southern Illinois University, Edwardsville, Edwardsville, IL 62026-1805, USA*

Received 5 August 2002; accepted 24 March 2003

Abstract

The periodic impact motions of passengers in a vehicle traveling on rough terrain are investigated through a linear model of vehicle and passenger systems. In this mechanical model, the human body is considered as a massless bar with a lumped mass. The linear model assumes that the motion response of vehicle is quite small compared to the passenger's pitch motion since the vehicle chassis has a quite large mass and large moment of inertia compared with each passenger. The period-1 motion pertaining to two impacts, respectively, on two walls during N-periods of the ground motion is predicted analytically and numerically. The stability and bifurcation of such a period-1 motion are determined. The impact motion becomes complicated with increasing ground motion amplitude, but the impact motion reduces with increasing torsional damping. Although the mechanical model used in this paper is an ideal one, the dynamic responses of the human body in vehicle traveling on rough terrain is useful for the rough evaluation of the human body safety in traveling vehicles.

1. Introduction

The human body motion in traveling vehicles is used to measure the human body comfort in vehicles, and the impact motion between the human body and vehicle is an important issue for us to discuss in order to measure passenger safety as well. In 1962, Coermann [1] considered the mechanical impedance of a human body in sitting and standing position at low frequency, and the human body response to the vehicle vibration was considered as an important factor in measuring comforts and safety in vehicles. In 1964, Wisner et al. [2] developed a biomechanical model of the human body with vehicle seat and suspension, and in 1969, Suggs et al. [3] developed a linear

*Corresponding author. Tel.: +1-618-650-5389; fax: +1-618-650-2555.
E-mail address: aluo@siue.edu (A.C.J. Luo).

0022-460X/03/$ - see front matter
doi:10.1016/S0022-460X(03)00417-6

damped–spring–mass model to investigate the vehicle seat vibration experimentally. The translational seat vibration to human body comfort was considered [4] in 1982. Ahmed and Goupillon [5] extended such research and developed an analytical model based on the tyre, cab and seat for predicting the ride vibration of an agricultural tractor. In 1999, Tewari and Prasad [6] considered a three-degrees-of-freedom system to model a tractor seat and operator system. The human body rotational response was not modelled. When the rotational motion of human body is considered, the equilibrium and stability of a non-linear vehicle and passenger system was investigated [7] in 2002, and it was observed that the number of impacts decrease with increasing stiffness of the rotational spring. However, the dynamic responses of the human body in a vehicle traveling on the rough terrain were not presented. In this paper, the periodic impact response of the human body in a traveling vehicle on the rough surface will be of interest since this impact motion will cause serious damage to the human body. This impact motion between the passengers (and/or drivers) and the vehicle cannot be investigated through continuous dynamic system theory. In recent decades, similar impact dynamical systems have been widely investigated (e.g., Refs. [8–17]). The impact motion in practice can be found in Refs. [8–12] and the stability, bifurcation and chaos for the impact motion were presented in Refs. [13–17]. The reason for analyzing a vehicle passenger impacting a front and rear wall due to steady state terrain induced pitching motions of a vehicle (the type of vehicle not revealed) is to find the ranges of parameters for driving safety and to improve the passenger seat design. Such ranges can be determined through the stability of period-1 impact motion. Once the impact between vehicles and passengers occurs, the passenger injuries can be measured through the energy transfer during impact.

In this paper, a linearized model for a three-degree-of-freedom passenger–vehicle system under terrain surface excitation is developed. Under periodic terrain surface excitation, the periodic impact response of the human body will be obtained analytically. The stability for such a periodic response will be investigated. The passenger impact responses based on the linear model will be simulated.

2. Mechanical model

A vehicle and passenger system consists of a chassis mass (rigid body) M, two suspensions mounted on the chassis and a mass m representing a passenger ($m \ll M$), as shown in Fig. 1. To simplify the mechanical model without losing the motion mechanism of the passenger in a vehicle with constant translation speed v, the passenger is modelled as a massless bar with length L rotating around point O′ plus a lumped mass at the other end. The distance between the mass center C and point O′ is e. The distances a_1 and a_2 are from point O′ to the right and left walls mounted on the vehicle, respectively. The distance from the chassis mass center to two suspensions is b. The torsional spring stiffness and damping coefficient are K_3 and C_3, respectively. Let $x(t)$ and $\psi(t)$ be the absolute vertical and angular displacements of chassis M; and $\theta(t)$ be the absolute angular displacement of passenger m. The free moving of the passenger between two walls is in the range determined by $-a_2/L \leqslant \sin(\theta - \psi) \leqslant a_1/L$, and the relative displacement is defined as

$$\Theta(t) = \theta(t) - \psi(t). \tag{1}$$

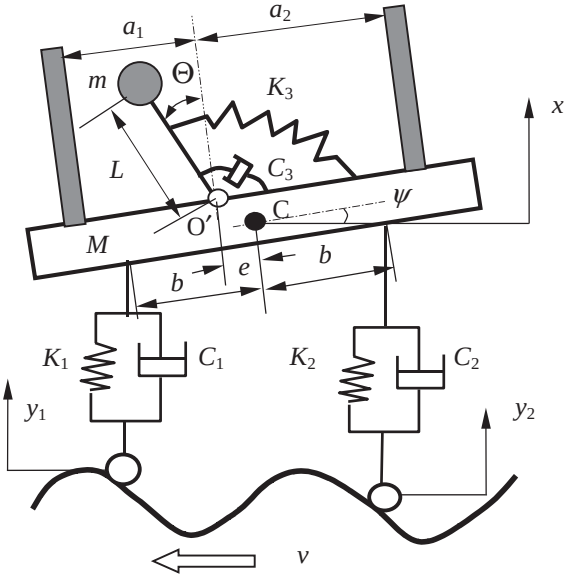

Fig. 1. Mechanical model for a vehicle and passenger system.

Consider a pavement surface

$$y_1 = \sum_{n=1}^{\infty} A_n \sin(\omega_n t + \varphi_n) \quad \text{and} \quad y_2 = \sum_{n=1}^{\infty} A_i \sin(\omega_n t + \varphi_n - \phi_n), \tag{2}$$

where A_n, ω_n and φ_n are the amplitude, frequency and phase angle of the nth term, respectively. The phase is $\phi_n = 2\omega_n b/v$ $(n = 1, 2, \ldots)$, where v is the transport speed of vehicle. A one-term expression for $\phi_1 = \phi\varphi_n = 0$ $(n \geqslant 2)$ is considered as an example, i.e.,

$$y_1 = A \sin \omega t \quad \text{and} \quad y_2 = A \sin(\omega t - \phi). \tag{3}$$

For $m \ll M$, the angular momentum conservation with respect to the chassis mass center gives approximately

$$(me^2 + J_M + mae)(\dot{\psi}^- - \dot{\psi}^+) + m(L^2 + ea)(\dot{\theta}^- - \dot{\theta}^+) = 0, \tag{4}$$

where the superscript dot represents the derivative with respect to time t. $\{\dot{\theta}^-, \dot{\psi}^-\}$ and $\{\dot{\theta}^+, \dot{\psi}^+\}$ are the angular velocities before and after impact, J_M is the moment of inertia for chassis with respect to the mass center, and $a \equiv \{a_1, a_2\}$. The impact law requires

$$\dot{\Theta}^+ = -\mu \dot{\Theta}^- \tag{5}$$

where μ is the coefficient of restitution. Eqs. (4) and (5) yield the velocity after impact

$$\dot{\theta}^+ = (1 - \eta)\dot{\theta}^- + \eta\dot{\psi}^- \quad \text{and} \quad \dot{\psi}^+ = (1 - \xi)\dot{\psi}^- + \xi\dot{\theta}^-, \tag{6}$$

where $\xi = (1 + \mu)\Delta_1/\Delta$, $\eta = (1 + \mu)\Delta_2/\Delta$, $\Delta_1 = mL^2 + mea$, $\Delta_2 = J_M + me^2 + mea$ and $\Delta = \Delta_1 + \Delta_2$.

As in Ref. [7], Lagrange's equation gives equations of motion for a vehicle and passenger system, i.e.,

$$(M+m)\ddot{x} - me\ddot{\psi}\cos\psi - mL\ddot{\theta}\sin\theta + (C_1+C_2)\dot{x} - mL\dot{\theta}^2\cos\theta - (C_1-C_2)b\dot{\psi}\cos\psi + (K_1+K_2)x - (K_1-K_2)b\sin\psi + me\dot{\psi}^2\sin\psi = C_1\dot{y}_1 + C_2\dot{y}_2 + K_1y_1 + K_2y_2 - (M+m)g, \quad (7)$$

$$(me^2+J_M)\ddot{\psi} + meL\ddot{\theta}\sin(\theta-\psi) - me\ddot{x}\cos\psi + C_3\dot{\psi} - C_3\dot{\theta} - (C_1-C_2)b\dot{x}\cos\psi + (C_1+C_2)b^2\dot{\psi}\cos^2\psi + K_3\psi - K_3\theta - (K_1-K_2)bx\cos\psi + meL\dot{\theta}^2\cos(\theta-\psi) = (C_2\dot{y}_2 - C_1\dot{y}_1)b\cos\psi - (K_1y_1 - K_2y_2)b\cos\psi + mge\cos\psi - (K_1+K_2)b^2\cos\psi\sin\psi, \quad (8)$$

$$mL^2\ddot{\theta} - mL\ddot{x}\sin\theta + meL\ddot{\psi}\sin(\theta-\psi) + C_3(\dot{\theta}-\dot{\psi}) + K_3\theta - K_\theta\psi - meL\dot{\psi}^2\cos(\theta-\psi) = mgL\sin\theta \quad (9)$$

with constraints in Eq. (6) at $\sin(\theta-\psi) = a_1/L$ (or $-a_2/L$).

In the linear model, the vehicle pitch is relatively small compared to the passenger rotation (i.e., $|\psi| \ll |\theta| < 1$). Since $\psi \ll \theta$, we have $\Theta \approx \theta$, thus $-a_2/L \leqslant \sin\theta \leqslant a_1/L$. In practice, $\theta \ll 1$ may not hold. To reduce difficulty of analysis, this assumption $\theta \ll 1$ will be used in this paper. Since both chassis mass and the moment of inertia are very large, from numerical simulation [7] it is observed that the responses of a vehicle to rough terrain are very small compared to the passenger's response. Therefore,

$$m \ll M, \quad me^2 \ll J_M, \quad |x| \ll L|\theta|, \quad \sin\theta \approx \theta, \quad \cos\theta \approx 1, \quad \sin\psi \approx \psi, \quad \cos\psi \approx 1. \quad (10)$$

With Eq. (10), Eqs. (7)–(9) reduce to

$$M\ddot{x} + (C_1+C_2)\dot{x} - (C_1-C_2)b\dot{\psi} + (K_1+K_2)x - (K_1-K_2)b\psi \approx C_1\dot{y}_1 + C_2\dot{y}_2 + K_1y_1 + K_2y_2 - (M+m)g, \quad (11)$$

$$J_M\ddot{\psi} - (C_1-C_2)b\dot{x} + (C_1+C_2)b^2\dot{\psi} - (K_1-K_2)bx + (K_1+K_2)b^2\psi \approx (C_2\dot{y}_2 - C_1\dot{y}_1)b - (K_1y_1 - K_2y_2)b \quad (12)$$

and

$$mL^2\ddot{\theta} + C_3\dot{\theta} + (K_3 - mgL)\theta \approx C_3\dot{\psi} + K_3\psi. \quad (13)$$

The vehicle vibration described in Eqs. (11)–(13) is independent of the passenger motion. With Eq. (2), the solution for the vehicle vibration is approximated by

$$x(t) = \alpha_1\sin\omega t + \alpha_2\cos\omega t + \gamma_1 + \alpha_3e^{\lambda_1 t} + \alpha_4e^{\lambda_2 t} + \alpha_5e^{\lambda_3 t} + \alpha_6e^{\lambda_4 t},$$
$$\psi(t) = \beta_1\sin\omega t + \beta_2\cos\omega t + \gamma_2 + \beta_3e^{\lambda_1 t} + \beta_4e^{\lambda_2 t} + \beta_5e^{\lambda_3 t} + \beta_6e^{\lambda_4 t}, \quad (14)$$

where the coefficients are presented in Appendix A.

For such a vehicle system, the transient motion decays rapidly since the vehicle damping is very large. For instance, consider system parameters ($M = 1200\,\text{kg}$, $J_M = 2500\,\text{kg m}^2$, $K_1 = 30\,\text{kN/m}$, $K_2 = 40\,\text{kN/m}$ and $C_1 = C_2 = 4\,\text{kN s/m}$), we have $\lambda_{1,2} \approx -3.25 \pm 6.95\text{i}$ and $\lambda_{3,4} \approx -2.20 \pm 5.37\text{i}$, where $\text{i} = \sqrt{-1}$. The exponential terms in Eq. (13) decrease rapidly with increasing time. For long enough time, the exponential terms in the vehicle vibration can be ignored. The steady state motion of the vehicle motion plays an impotent role in the passenger's motion. Thus, under the

steady state vehicle motion, the passenger pitch motion is obtained through Eq. (13) is

$$\theta(t) = A_1^* \sin \omega t + A_2^* \cos \omega t + A_3^* + A_4 e^{\lambda_1 (t-t_0)} + A_5 e^{\lambda_2 (t-t_0)}, \tag{15}$$

where t_0 is the initial time and other parameters A_1^*, A_2^*, A_3^* are listed in Appendix A. The parameters A_4, A_5 are determined through the initial condition.

3. Period-1 motion and stability

Passengers' periodic responses in a vibrating vehicle are a key to obtain other responses. Herein, the period-1 impact motion is that the passenger moves from one constraint wall to another and turns back during N-periods of the ground motion. Once the period-1 motion is obtained, the other complicated motion can be numerically simulated. For the initial condition not being at one of the constraint walls (e.g., the passenger sits upright without any relative velocity), the solution can be transferred to the first impact on one of the constraint walls. The velocity and location for such impact time can be used as a new initial condition. When the new initial condition is obtained, the procedure presented in this section can be used. Note that the initial condition is at time $t = t_0$ instead of $t = 0$, and the solution based on this initial condition is more general. The advantage of this solution expression lies in obtaining iterative mapping relations. Therefore, in this section, the solution for period-1 motion will be developed for a specified initial time t_0. The procedure for achieving mapping equations from a constraint wall to another is presented as follows.

With Eq. (1), the constraints of the impact walls become

$$\Theta_{r1} = \arcsin(a_1/L), \quad \Theta_{r2} = -\arcsin(a_2/L). \tag{16}$$

Furthermore, for $\Theta_{r2} \leqslant \Theta(t) \leqslant \Theta_{r1}$, Eq. (15) becomes

$$\Theta(t) = A_1 \sin \omega t + A_2 \cos \omega t + A_3 + A_4 e^{\lambda_1 (t-t_0)} + A_5 e^{\lambda_2 (t-t_0)} \tag{17}$$

and the corresponding constants are $A_1 = (A_1^* - \beta_1)$, $A_2 = (A_2^* - \beta_2)$, $A_3 = (A_3^* - \gamma_2)$. The constants A_4 and A_5 are functions of initial displacement, initial velocity and the initial time t_0, i.e., $A_4(\Theta_0, \dot{\Theta}_0, t_0)$ and $A_5(\Theta_0, \dot{\Theta}_0, t_0)$.

From Eq. (16), the impact law in Eq. (4) becomes

$$\dot{\Theta}^+ = -\mu_j \dot{\Theta}^- \quad \text{at } \Theta = \{\Theta_{rj}, j = 1, 2\}. \tag{18}$$

where μ_1 and μ_2 are the restitution coefficient of impact on the wall-1 (the front wall) and wall-2 (the back wall). To determine the periodic response of a passenger, after the ith impact, the initial conditions selected on the wall-1 (the front wall) is

$$\Theta^{(i)}(t_i) = \Theta_{r1}, \quad \dot{\Theta}^{(i)}(t_i) = \dot{\Theta}_i^+ \quad \text{and} \quad t = t_i. \tag{19}$$

The motion response between the wall-1 to wall-2 is given by

$$\Theta^{(i)}(t) = A_1 \sin \omega t + A_2 \cos \omega t + A_3 + A_4^{(i)} e^{\lambda_1 (t-t_i)} + A_5^{(i)} e^{\lambda_2 (t-t_i)}, \tag{20}$$

where

$$A_4^{(i)}(\Theta_{rj},\dot{\Theta}_i,t_i)=\frac{1}{\lambda_2-\lambda_1}\left[(\Theta_{rj}\lambda_2-\dot{\Theta}_i-A_3\lambda_2)-(A_2\lambda_2-A_1\omega)\cos\omega t_i-(A_1\lambda_2+A_2\omega)\sin\omega t_i\right],$$

$$A_5^{(i)}(\Theta_{rj},\dot{\Theta}_i,t_i)=\frac{1}{\lambda_1-\lambda_2}\left[(\Theta_{rj}\lambda_1-\dot{\Theta}_i-A_3\lambda_1)-(A_2\lambda_1-A_1\omega)\cos\omega t_i-(A_1\lambda_1+A_2\omega)\sin\omega t_i\right]. \tag{21}$$

At time t_{i+1}, another impact between the passenger and vehicle occurs. Just before impact, we have

$$\Theta^{(i)}(t_{i+1})=\Theta_{r2}=A_1\sin\omega t_{i+1}+A_2\cos\omega t_{i+1}+A_3+A_4^{(i)}e^{\lambda_1(t_{i+1}-t_i)}+A_5^{(i)}e^{\lambda_2(t_{i+1}-t_i)} \tag{22}$$

and

$$\dot{\Theta}^{(i)}(t_{i+1})=\dot{\Theta}_{i+1}^{-}=A_1\omega\sin\omega t_{i+1}-A_2\omega\cos\omega t_{i+1}+A_4^{(i)}\lambda_1e^{\lambda_1(t_{i+1}-t_i)}+A_5^{(i)}\lambda_2e^{\lambda_2(t_{i+1}-t_i)}. \tag{23}$$

The occurrence of impact requires

$$\dot{\Theta}_{i+1}^{+}=-\mu_2\dot{\Theta}_{i+1}^{-}. \tag{24}$$

Similarly, after the $(i+1)$th impact, the initial condition for the $(i+1)$th movement of passenger is

$$\Theta^{(i+1)}(t_{i+1})=\Theta_{r2},\quad \dot{\Theta}^{(i+1)}(t_{i+1})=\dot{\Theta}_{i+1}^{+}\quad\text{and}\quad t=t_{i+1}. \tag{25}$$

The passenger motion from the wall-2 back to the wall-1 is

$$\Theta^{(i+1)}(t)=A_1\sin\omega t+A_2\cos\omega t+A_3+A_4^{(i+1)}e^{\lambda_1(t-t_{i+1})}+A_5^{(i+1)}e^{\lambda_2(t-t_{i+1})}. \tag{26}$$

Just before the second impact between the passenger and vehicle occurs on wall-1, the time $t=t_{i+2}$ and Eq. (26) leads to

$$\Theta^{(i+1)}(t_{i+2})=\Theta_{r1}=A_1\sin\omega t_{i+2}+A_2\cos\omega t_{i+2}+A_3+A_4^{(i+1)}e^{\lambda_1(t_{i+2}-t_{i+1})}+A_5^{(i+1)}e^{\lambda_2(t_{i+2}-t_{i+1})} \tag{27}$$

and

$$\dot{\Theta}^{(i+1)}(t_{i+2})=\dot{\Theta}_{i+2}^{-}=A_1\omega\sin\omega t_{i+2}-A_2\omega\cos\omega t_{i+2}+A_4^{(i+1)}\lambda_1e^{\lambda_1(t_{i+2}-t_{i+1})}+A_5^{(i+1)}\lambda_2e^{\lambda_2(t_{i+2}-t_{i+1})}. \tag{28}$$

The impact constraint at time t_{i+2} requires

$$\dot{\Theta}_{i+2}^{+}=-\mu_1\dot{\Theta}_{i+2}^{-}. \tag{29}$$

Substitution of Eq. (24) into Eqs. (22) and (23), and Eq. (29) into Eqs. (27) and (28), respectively generates the forward map from the wall-1 to the wall-2 ($P_f:(t_i,\Theta_i)\to(t_{i+1},\Theta_{i+1})$) and the return map from wall-2 to wall-1 ($P_r:(t_{i+1},\Theta_{i+1})\to(t_{i+2},\Theta_{i+2})$), the maps form the Poincare mapping $P=P_r\circ P_f:(t_i,\Theta_i)\to(t_{i+2},\Theta_{i+2})$.

$$\begin{aligned}P_f:\ t_{i+1}&=f_1(t_i,\dot{\Theta}_i,\mu_2),\quad \dot{\Theta}_{i+1}=f_2(t_i,\dot{\Theta}_i,\mu_2),\\ P_r:\ t_{i+2}&=f_1(t_{i+1},\dot{\Theta}_{i+1},\mu_1),\quad \dot{\Theta}_{i+2}=f_2(t_{i+1},\dot{\Theta}_{i+1},\mu_1).\end{aligned} \tag{30}$$

Consider the period-1 motion in an N period of the ground motion, i.e., the period-1 motion from time t_i to t_{i+2} during an N period of the ground motion needs the following conditions:

$$t_{i+2} = t_i + NT \quad \text{and} \quad \Theta^+_{i+2} = \Theta^+_i, \tag{31}$$

where N is an integer and $T = 2\pi/\omega$. For convenience, the superscript $(+)$ will be dropped from now on. Using Eqs. (22)–(24) and (27)–(29) yields

$$\begin{aligned}
&A_1 \sin \omega t_{i+1} + A_2 \cos \omega t_{i+1} + A_3 + A_4^{(i)} e^{\lambda_1 (t_{i+1} - t_i)} + A_5^{(i)} e^{\lambda_2 (t_{i+1} - t_i)} - \Theta_{r2} = 0,\\
&-\mu_2 (A_1 \omega \sin \omega t_{i+1} - A_2 \omega \cos \omega t_{i+1} + A_4^{(i)} \lambda_1 e^{\lambda_1 (t_{i+1} - t_i)} + A_5^{(i)} \lambda_2 e^{\lambda_2 (t_{i+1} - t_i)}) - \dot{\Theta}_{i+1} = 0,\\
&A_1 \sin \omega t_i + A_2 \cos \omega t_i + A_3 + A_4^{(i+1)} e^{\lambda_1 (t_i + NT - t_{i+1})} + A_5^{(i+1)} e^{\lambda_2 (t_i + NT - t_{i+1})} - \Theta_{r1} = 0,\\
&-\mu_1 (A_1 \omega \sin \omega t_i - A_2 \omega \cos \omega t_i + A_4^{(i+1)} \lambda_1 e^{\lambda_1 (t_i + NT - t_{i+1})} + A_5^{(i+1)} \lambda_2 e^{\lambda_2 (t_i + NT - t_{i+1})}) - \dot{\Theta}_i = 0.
\end{aligned} \tag{32}$$

Solving Eq. (32) yields the solutions $(t_i, \dot{\Theta}_i, t_{i+1}, \dot{\Theta}_{i+1})$ for the pioed-1 motion. Once the period-1 motion is obtained, the stability and bifurcation will be investigated through the linearization of Eq. (30). Using the chain rules of derivatives, the Jacobian matrix gives

$$\begin{pmatrix} \Delta t_{i+2} \\ \Delta \dot{\Theta}_{i+2} \end{pmatrix} = [DP] \begin{pmatrix} \Delta t_i \\ \Delta \dot{\Theta}_i \end{pmatrix} = [DP_r]_{(t_{i+1}, \dot{\Theta}_{i+1})} [DP_f]_{(t_i, \dot{\Theta}_i)} \begin{pmatrix} \Delta t_i \\ \Delta \dot{\Theta}_i \end{pmatrix}, \tag{33}$$

where

$$[DP_r] = \begin{bmatrix} \dfrac{\partial t_{i+2}}{\partial t_{i+1}} & \dfrac{\partial t_{i+2}}{\partial \dot{\Theta}^+_{i+1}} \\ \dfrac{\partial \dot{\Theta}_{i+2}}{\partial t_{i+1}} & \dfrac{\partial \dot{\Theta}_{i+2}}{\partial \dot{\Theta}_{i+1}} \end{bmatrix} \quad \text{and} \quad [DP_f] = \begin{bmatrix} \dfrac{\partial t_{i+1}}{\partial t_i} & \dfrac{\partial t_{i+1}}{\partial \dot{\Theta}_i} \\ \dfrac{\partial \dot{\Theta}_{i+1}}{\partial t_i} & \dfrac{\partial \dot{\Theta}_{i+1}}{\partial \dot{\Theta}_i} \end{bmatrix}. \tag{34}$$

The components in Eq. (34) are computed in Appendix A. The stability of the period-1 impact motion is determined through the two eigenvalues of the mapping, computed by

$$|[DP] - \lambda \mathbf{I}| = 0. \tag{35}$$

The eigenvalues of a fixed point of the periodi-1 motion mapping are expressed by $\lambda_{1,2} = \mathrm{Re}(\lambda) \pm \mathrm{iIm}(\lambda)$, where $\mathrm{i} = \sqrt{-1}$. For $|\lambda_k| < 1$ $(k = 1, 2)$, such a fixed point is a stable focus, and for $|\lambda_k| > 1$ $(k = 1$ or $2)$, the fixed point is an unstable focus. If $|\lambda_{1(\mathrm{or}2)}| = +1$ with complex numbers, the Neimark bifurcation occurs. For two real eigenvalues, the stable node requires $\max_{k=1,2}(|\lambda_k|) < 1$, and the unstable node (or saddle) requires $\max_{k=1,2}(|\lambda_k|) > 1$. The saddle of the first kind is $\max_{k=1,2}(\lambda_k) > 1$ and the saddle of the second kind needs $\min_{k=1,2}(\lambda_k) < -1$. If one of the two eigenvalues is -1 (or $\lambda_{1(\mathrm{or}2)} = -1$), the period doubling bifurcation occurs. If one of the two eigenvalues is $+1$ (or $\lambda_{1(\mathrm{or}2)} = +1$), the first saddle-node bifurcation occurs.

4. Illustrations

To verify the approximate analytical analysis, a numerical investigation of passenger–vehicle systems follows. Consider a set of system parameters ($M = 1200\,\text{kg}$, $m = 150\,\text{kg}$, $J_M = 2500\,\text{kgm}^2$, $C_1 = C_2 = 4\,\text{kN s/m}$, $K_1 = 30\,\text{kN/m}$, $K_2 = 40\,\text{kN/m}$, $K_3 = 400\,\text{N/m}$, $L = 0.6\,\text{m}$, $a_1 = 0.5\,\text{m}$, $a_2 = 0.3\,\text{m}$), a ground sinusoidal wavelength $B = 10\,\text{m}$, the vehicle's velocity $v = 10\,\text{m/s}$, and impact restitution coefficients $\mu_1 = \mu_2 = 0.8$. Using the given parameters, the period of the ground motion is $T = 2\pi/\omega = B/v = 1\,\text{s}$. Note that from those parameters we have $-1 < \theta_{r1} < \Theta_{r1} \approx 0.9851 < 1$ and $-1 < \Theta_{r2} \approx -0.5236 < \theta_{r2} < 1$, not satisfying assumptions in Eq. (10) perfectly, but it is good enough for a qualitative estimate of passenger motions. Once the length L increases, the prediction of passenger motions given in this section will be much closer to the realistic model. The impact phase is expressed by $\varphi_i = \omega t_i$. In the analytical prediction, for small ground excitations, the difference between φ_i and φ_{i+1} is close to π for $N = 1$. With increasing surface amplitude, the time interval $(t_{i+1} - t_i)$ becomes smaller and smaller, but the time interval $(t_{i+2} - t_{i+1})$ increases. From Eq. (32), the corresponding solutions to the period-1 motion $(t_i, \dot{\Theta}_i, t_{i+1}, \dot{\Theta}_{i+1})$ are obtained, and the solution $(t_i, \dot{\Theta}_i)$ is as the initial impact conditions for the numerical simulation of such a periodic impact motion. The numerical predictions are computed through Eq. (13) with an adaptive Runge–Kutta integration scheme.

The numerical and analytical results of the impact phase and impact velocity are presented in the (a) and (b) plots of Figs. 2–4, respectively. The dark solid curves are the stable period-1 motion predicted by the analytical model, and the dashed curves are the unstable period-1 impact motion. The numerical predictions are denoted by small dots. In the (c) and (d) plots of Figs. 2–4, the real and imaginary parts for the corresponding eigenvalues of the analytical solutions of period-1 impact motion are illustrated. The results for non-damping case are plotted in Fig. 2. The ground motion amplitude ranges for the stable period-1 impact are from $A \approx 0.062$ to $0.44\,\text{m}$ (analytical) but from $A \approx 0.064$ to $0.441\,\text{m}$ (numerical). It is observed that the numerical and analytical predictions of the initial phase agree well. From the eigenvalues $\lambda_i (i = 1, 2)$ for the analytical period-1 motion in the (c) and (d) plots of Fig. 2, the critical values are: $A_{cr1} \approx 0.064\,\text{m}$, $A_{cr2} \approx 0.066\,\text{m}$, $A_{cr3} \approx 0.141\,\text{m}$, $A_{cr4} \approx 0.201\,\text{m}$, $A_{cr5} \approx 0.433\,\text{m}$ and $A_{cr6} \approx 0.44\,\text{m}$. At $A = A_{cr1}$, the saddle-node bifurcation of the first kind occurs. For $A < A_{cr1}$, no period-1 impact motion exists. The impact motion is around the wall-1 (or wall-2), and the impact phase can be from 0 to 2π. However, in Fig. 2(b), it is observed that the impact velocity is almost zero in the range of $A < A_{cr1}$. This implies that the human body does not have any large amplitude motion. When the passenger sits upright without consideration of human factors, the human body, like a corpse, has small amplitude motion near $\theta = 0$. Once human factors are considered, the live passenger can adjust by him/herself and stay in a position without any significant relative velocity. In this case ($C_3 = 0$), the passenger is safe in vehicles running on the rough terrain possessing a sinusoidal surface amplitude $A < A_{cr1} = 0.062$.

For $A > A_{cr1}$, the impact motions between vehicle and passenger appear. For the three ground motion amplitude ranges ($A_{cr1} < A < A_{cr2}$, $A_{cr3} < A < A_{cr4}$ and $A_{cr5} < A < A_{cr6}$), the period-1 impact motion is a stable node since the corresponding eigenvalues are real and less than one. For the two amplitude range ($A_{cr2} < A < A_{cr3}$ and $A_{cr4} < A < A_{cr5}$), the period-1 impact motion is stable focus because the eigenvalues are complex and their magnitudes are less than one. At $A = A_{cr6}$, the period doubling bifurcation occurs since one of the two eigenvalues is –1. For $A > A_{cr6}$, the

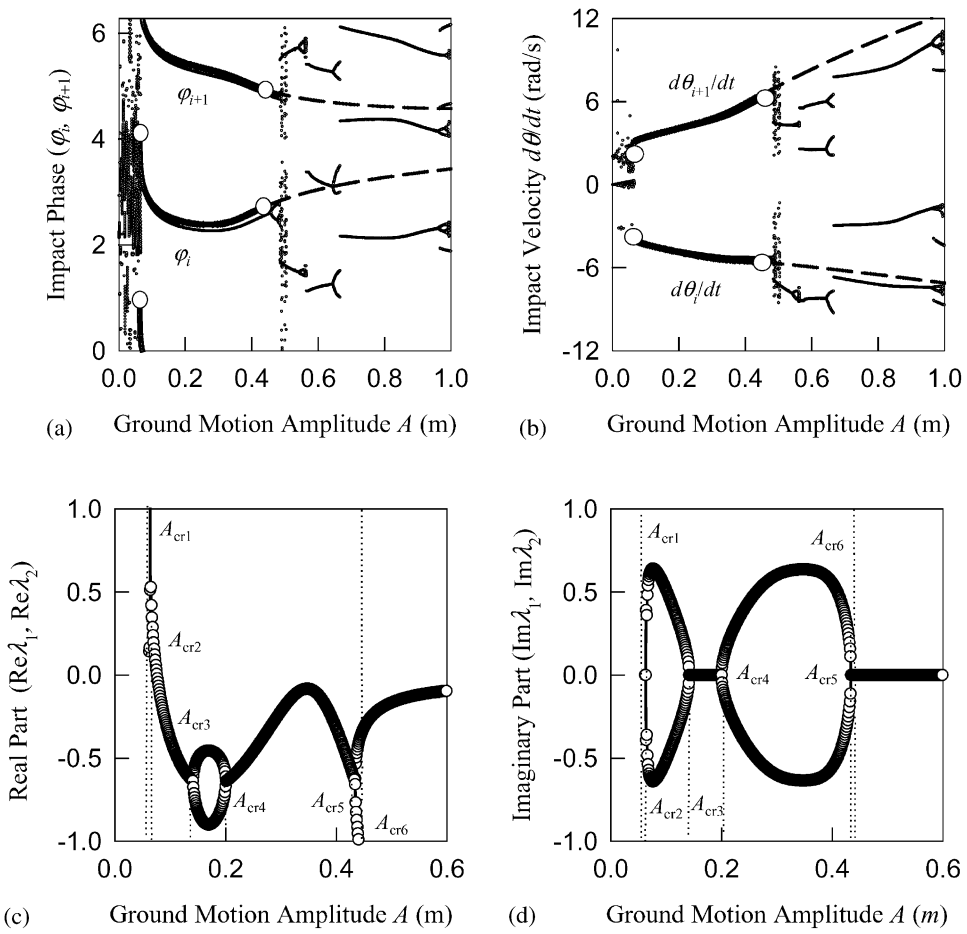

Fig. 2. Analytical and numerical predictions of: (a) impact phase, (b) impact velocity, (c) real part and (d) imaginary part of the eigenvalues for the analytical solution of perioid-1 impact motion ($C_3 = 0$) with parameter $M = 1200$ kg, $m = 150$ kg, $J_M = 2500\,\mathrm{kg\,m^2}$, $C_1 = C_2 = 4$ kN s/m, $K_1 = 30$ kN/m, $K_2 = 40$ kN/m, $K_3 = 400$ N/m, $L = 0.6$ m, $a_1 = 0.5$ m, $a_2 = 0.3$ m, ground sinusoidal wavelength $B = 10$ m, vehicle's velocity $v = 10$ m/s, and impact restitution coefficients $\mu_1 = \mu_2 = 0.8$.

perod-1 impact motion becomes unstable. From the numerical prediction, we have $A_{cr1} = 0.067$ m and $A_{cr6} = 0.441$ m. Under a small amplitude ground motion, live passengers can control their motion for such a period-1 motion to avoid impacts between the vehicle and human body. With increasing ground motion amplitude, the impact motion cannot be avoided since the passengers will lose control of their motion. In this case, the motion of the human body will be like a corpse sitting in the vibrating vehicle.

If $A > A_{cr6}$, other periodic impact motions and chaotic motions may appear. For $A_{cr6} < A < A_{cr7}$ ($A_{cr7} \approx 0.478$m), the period-2 impact motion exists. At $A = A_{cr7}$, the period-doubling bifurcation of the period-2 impact motion occurs. For $A_{cr8} < A < A_{cr9}$ ($A_{cr8} \approx 0.501$ m and $A_{cr9} \approx 0.537$ m), there is another period-1 impact motion that is not given by the analytical prediction. This is

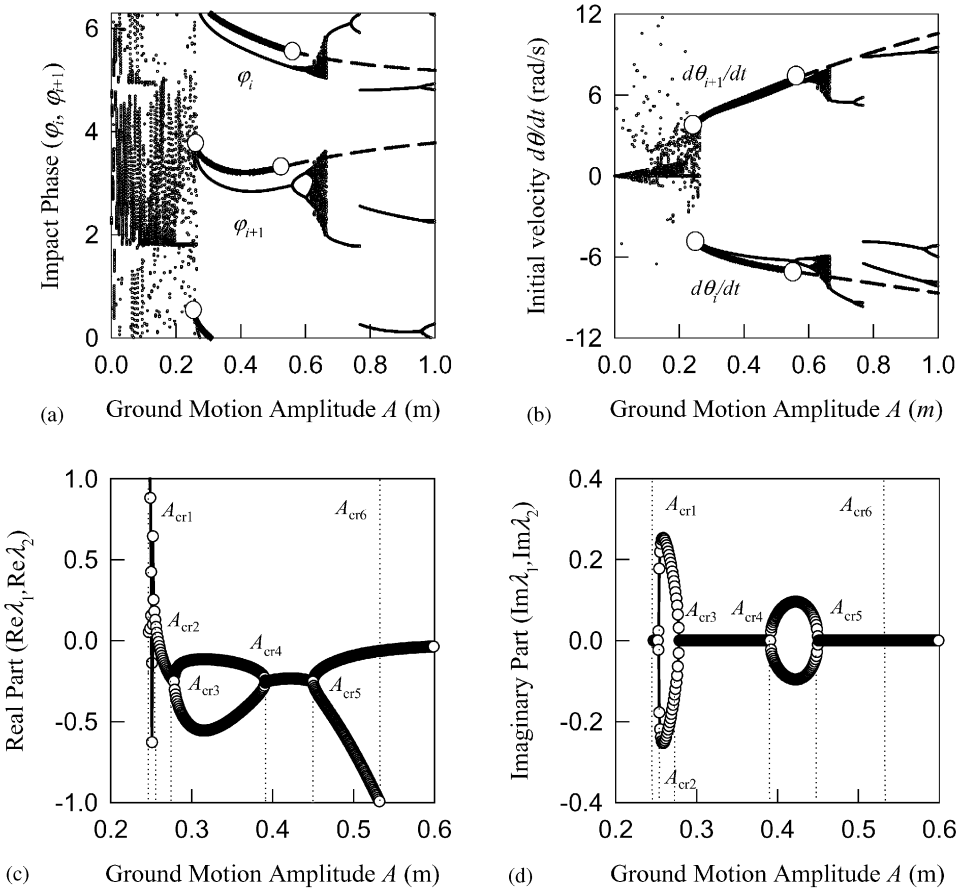

Fig. 3. Analytical and numerical predictions of: (a) impact phase, (b) impact velocity, (c) real part and (d) imaginary part of the eigenvalues for the analytical solution of perioid-1 impact motion ($C_3 = 100\,\mathrm{N\,m\,s/rad}$) with parameters: $M = 1200\,\mathrm{kg}$, $m = 150\,\mathrm{kg}$, $J_M = 2500\,\mathrm{kg\,m^2}$, $C_1 = C_2 = 4\,\mathrm{kN\,s/m}$, $K_1 = 30\,\mathrm{kN/m}$, $K_2 = 40\,\mathrm{kN/m}$, $K_3 = 400\,\mathrm{N/m}$, $L = 0.6\,\mathrm{m}$, $a_1 = 0.5\,\mathrm{m}$, $a_2 = 0.3\,\mathrm{m}$, ground sinusoidal wavelength $B = 10\,\mathrm{m}$, vehicle's velocity $v = 10\,\mathrm{m/s}$, and impact restitution coefficients $\mu_1 = \mu_2 = 0.8$.

because the solutions of the non-linear algebraic equations (32) are convergent to one of the possible period-1 solution. If $A_{cr10} \leqslant A \leqslant A_{cr12}$ ($A_{cr10} \approx 0.565\,\mathrm{m}$ and $A_{cr12} \approx 0.651\,\mathrm{m}$), the impact model switches to a new model relative to one impact on wall-1 and two continuous impacts on wall-2. In this range, only one period doubling bifurcation occurs at $A_{cr11} \approx 0.627\,\mathrm{m}$, and the impact motion model switches to a model pertaining to two continuous impacts on wall-1 and one impact on wall-2. The period-1 motion for such a model exists in the range of $A_{cr12} < A \leqslant A_{cr13} \approx 0.981\,\mathrm{m}$.

For a damping case ($C_3 = 100\,\mathrm{N\,m\,s/rad}$), the numerical and analytical predictions of the impact motion, and the real and imaginary parts of the corresponding eigenvalues for the analytical period-1 motion are presented in Fig. 3. Compared to the non-damping case, the critical values for the analytical period-1 impact motion are: $A_{cr1} \approx 0.2508\,\mathrm{m}$, $A_{cr2} \approx 0.253\,\mathrm{m}$, $A_{cr3} \approx 0.279\mathrm{m}$, $A_{cr4} \approx 0.392\,\mathrm{m}$, $A_{cr5} \approx 0.451\,\mathrm{m}$ and $A_{cr6} \approx 0.533\,\mathrm{m}$. The errors of the impact phase and velocity given by the two

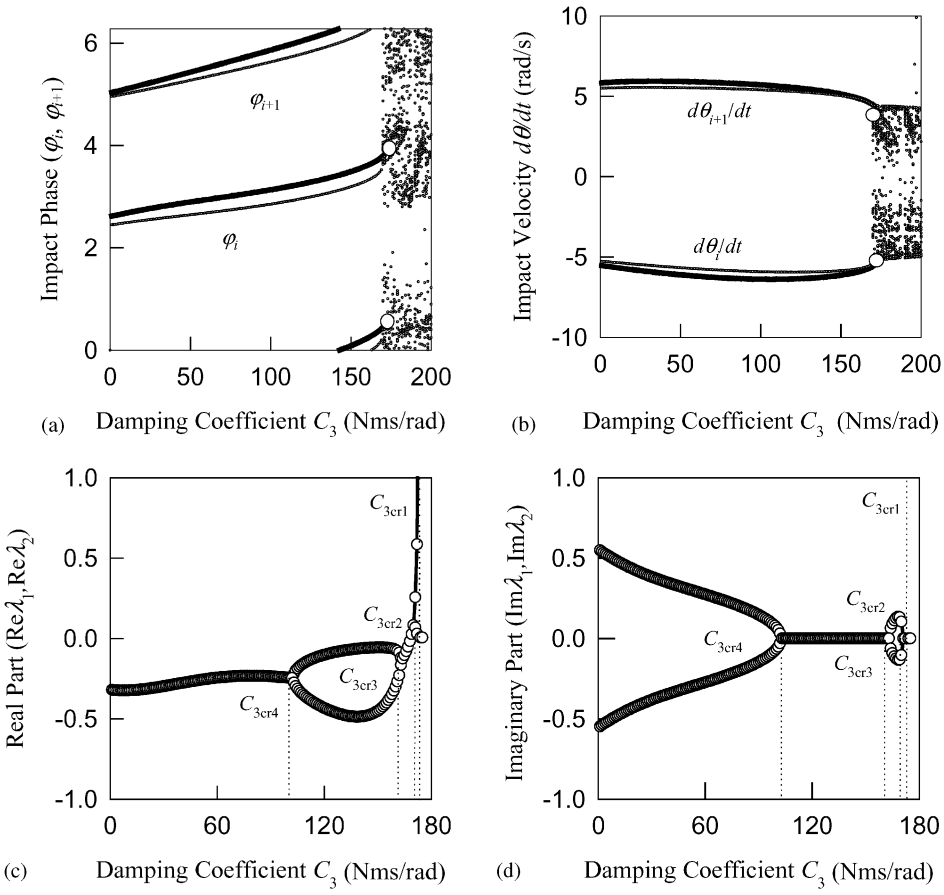

Fig. 4. Analytical and numerical predictions of: (a) impact phase, (b) impact velocity, (c) real part and (d) imaginary part of the eigenvalues for the analytical solution of perioid-1 impact motion ($A = 0.4$ m) with parameters: $M = 1200$ kg, $m = 150$ kg, $J_M = 2500\,\mathrm{kg\,m^2}$, $C_1 = C_2 = 4$ kN s/m, $K_1 = 30$ kN/m, $K_2 = 40$ kN/m, $K_3 = 400$ N/m, $L = 0.6$ m, $a_1 = 0.5$ m, $a_2 = 0.3$ m, ground sinusoidal wavelength $B = 10$ m, vehicle's velocity $v = 10$ m/s, and impact restitution coefficients $\mu_1 = \mu_2 = 0.8$.

predictions for this case are larger than the non-damping case. The numerical prediction gives: $A_{cr1} \approx 0.262$ m, $A_{cr6} \approx 0.543$ m, $A_{cr7} \approx 0.594$ m, $A_{cr7} \approx 0.667$ m, $A_{cr9} \approx 0.741$ m, $A_{cr10} \approx 0.769$ m and $A_{cr11} \approx 0.957$ m. The range for the period-1 motions of the stable node kind becomes larger, but the total range for the stable period-1 motion becomes smaller. Because of the existence of seat damping, the motion with almost zero velocity around the wall-1 (or wall-2) has a large range for the ground motion amplitude compared to the non-damping case. This implies that the safety of passengers responding to the ground motion amplitude with damping is higher than without damping. Again, if a passenger sits upright with small relative motion, when human factors are considered, such a small motion of passengers can be adjusted by human body. The real and imaginary parts of eigenvalues for this case are plotted in Figs. 3(c) and (d), respectively.

From the foregoing analysis, damping is a key factor for changing the stability condition. The impact phase and velocity versus the damping coefficient is discussed, as illustrated in Fig. 4 for

$A = 0.4$ m. The stability and bifurcation analysis gives the critical values as $C_{3cr1} \approx 173$ N m s/rad, $C_{3cr2} \approx 170$ N m s/rad, $C_{3cr3} \approx 163$ N m s/rad and $C_{3cr4} \approx 103$ N m s/rad. From these critical values, for the damping ranges ($C_{3cr2} < C_3 < C_{3cr1}$ and $C_{3cr4} < C_3 < C_{3cr3}$), the period-1 impact motion is a stable node, and for the damping ranges ($0 < C_3 < C_{3cr4}$, $C_{3cr3} < C_3 < C_{3cr2}$ and $C_{3cr4} < C_3 < C_{3cr3}$), the impact motion is stable focus. At $C_3 = C_{3cr1}$, the first saddle-node bifurcation for the period-1 impact motion occurs. The numerical prediction gives $C_{3cr1} \approx 169$ N m s/rad. In addition, it is observed that the impact motion will reduce with increasing damping. For $C_3 > C_{3cr1}$, the impact motion with almost zero-velocity on the wall-1 or the wall-2 occurs. Therefore, the passengers in vehicles traveling on the sinusoidal surface are safe in this range of damping. For a better understanding of the impact motion between the passengers and vehicle, analytical stability and bifurcation conditions for the period-1 impact motion are summarized in Fig. 5. In Fig. 5(d), the

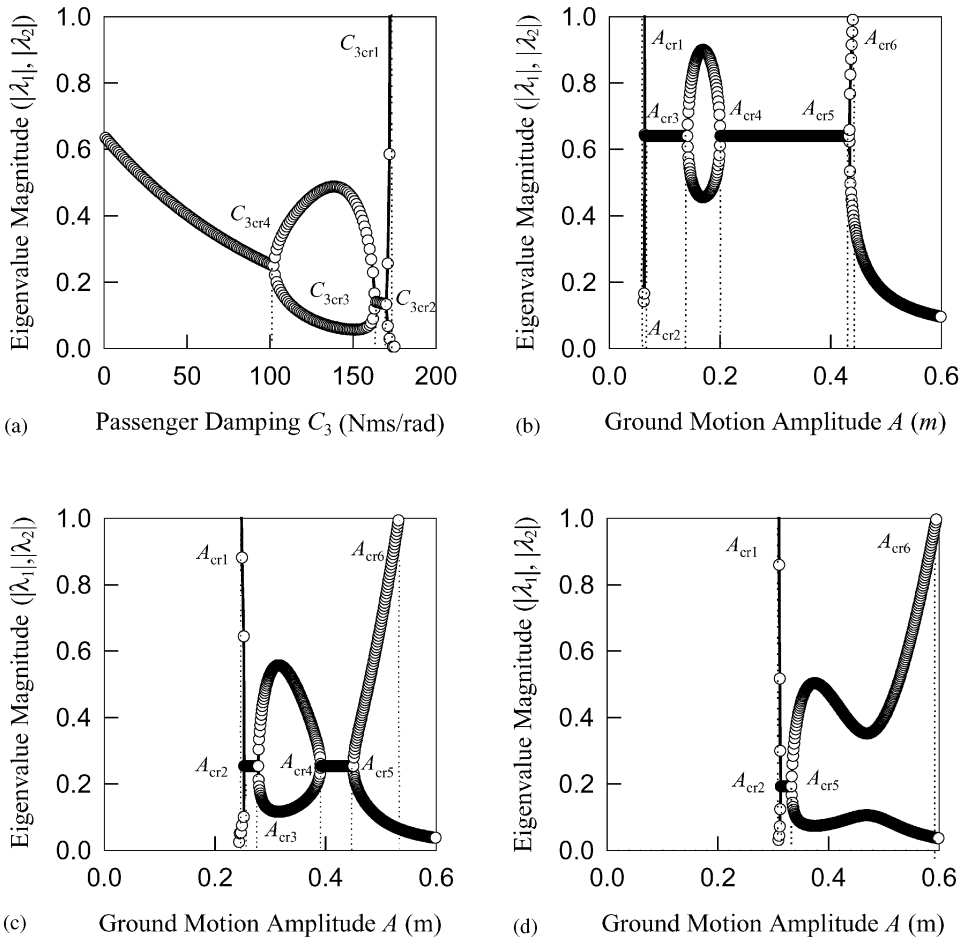

Fig. 5. Stability conditions ((a) $A = 0.4$ m, (b) $C_3 = 0$, (c) $C_3 = 100$ N m s/rad (d) $C_3 = 130$ N m s/rad) for the analytical solution of perioid-1 impact motion with parameter $M = 1200$ kg, $m = 150$ kg, $J_M = 2500$ kg m^2, $C_1 = C_2 = 4$ kN s/m, $K_1 = 30$ kN/m, $K_2 = 40$ kN/m, $K_3 = 400$ N/m, $L = 0.6$ m, $a_1 = 0.5$ m, $a_2 = 0.3$ m, ground sinusoidal wavelength $B = 10$ m, vehicle's velocity $v = 10$ m/s, and impact restitution coefficients $\mu_1 = \mu_2 = 0.8$.

critical values are: $A_{cr1} \approx 0.31$ m, $A_{cr2} \approx 0.314$ m, $A_{cr5} \approx 0.333$ m and $A_{cr6} \approx 0.595$ m for $C_3 = 130$ Nms/rad. The period-1 motion changes from the stable focus to node.

To observe the periodic impact motions for the simplified vehicle passenger system, the phase planes are illustrated for $C_3 = 0$ and 100 N m s/rad in Figs. 6 and 7, respectively. The quasi-symmetric period-1 impact motion is shown in Fig. 6(a) for $A = 0.1$ m. The quasi-symmetric, period-1 impact motion is defined as $t_{i+1} - t_i \approx t_{i+2} - t_{i+1}$ for the model of two impacts, respectively, on the two walls during an N-period (herein, $N = 1$ for demonstration). For $A = 0.4$ m, the phase plane for an asymmetrical period-1 impact motion is plotted in Fig. 6(b). The time intervals from wall-1 to wall-2 and returning back are distinguishing. As discussed before, for

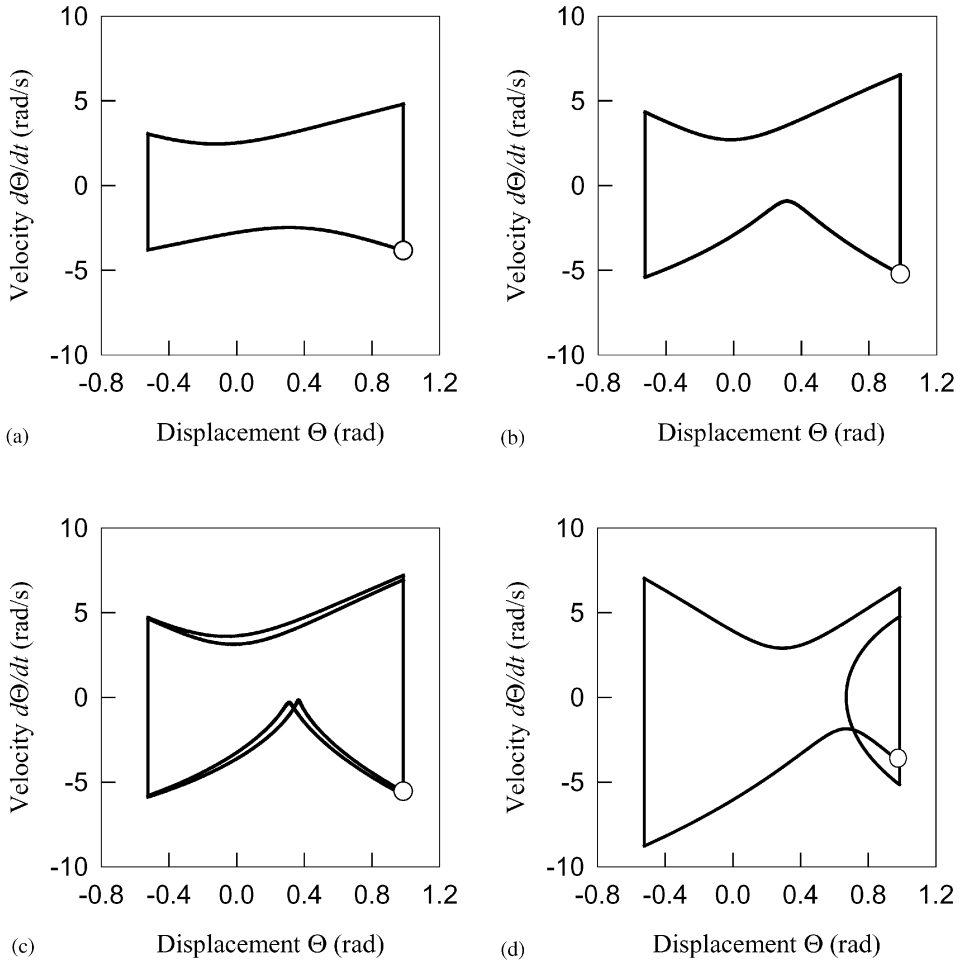

Fig. 6. Phase planes ($C_3 = 0$, $\theta = 0.9851$ rad) ((a) $A = 0.1$ m, $t_0 = 0.9187$ s and $\dot{\theta} = -4.2692$ rad/s; (b) $A = 0.4$ m, $t_0 = 0.7936$ s and $\dot{\theta} = -5.2655$ rad/s; (c) $A = 0.47$ m, $t_0 = 0.7655$ s and $\dot{\theta} = -5.4197$ rad/s; (d) $A = 0.8$ m, $t_0 = 0.7006$ s and $\dot{\theta} = -7.2166$ rad/s) for the analytical solution of perioid-1 impact motion with parameters: $M = 1200$ kg, $m = 150$ kg, $J_M = 2500$ kg m^2, $C_1 = C_2 = 4$ kN s/m, $K_1 = 30$ kN/m, $K_2 = 40$ kN/m, $K_3 = 400$ N/m, $L = 0.6$ m, $a_1 = 0.5$ m, $a_2 = 0.3$ m, ground sinusoidal wavelength $B = 10$ m, vehicle's velocity $v = 10$ m/s, and impact restitution coefficients $\mu_1 = \mu_2 = 0.8$.

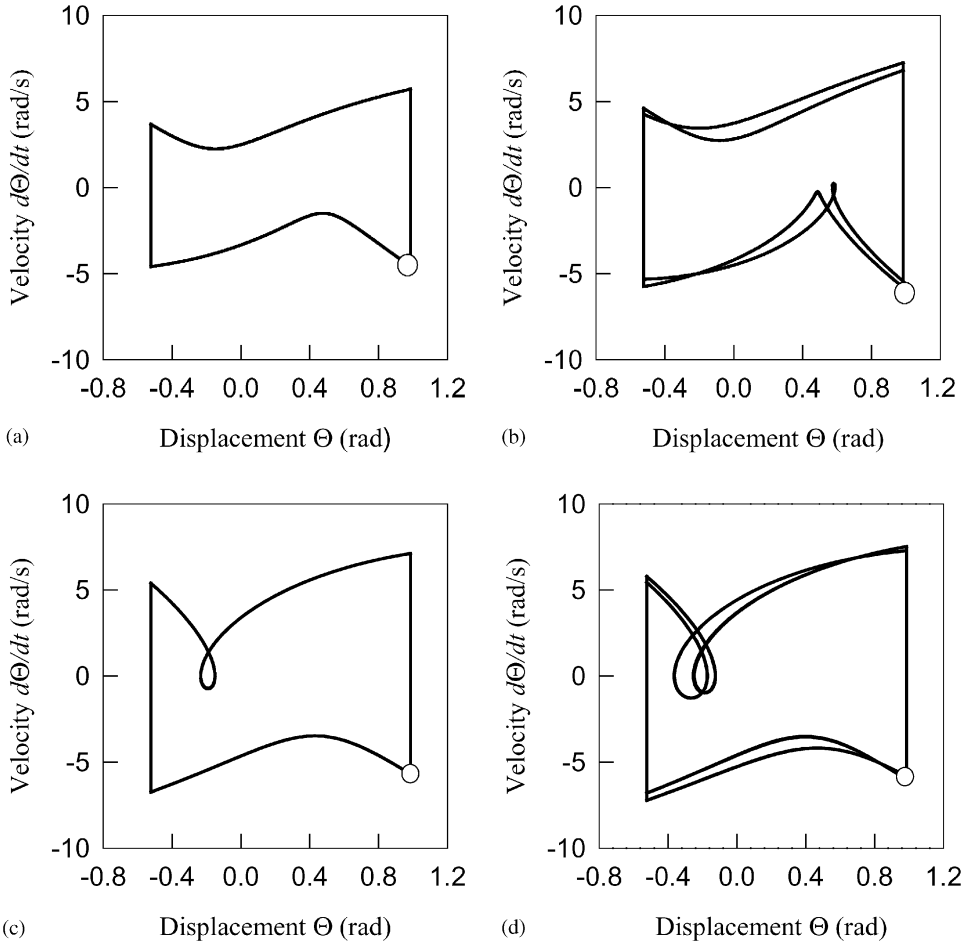

Fig. 7. Phase planes ($C_3 = 100\,\mathrm{N\,m\,s/rad}$, $\theta = 0.9851\,\mathrm{rad}$) ((a) $A = 0.4\,\mathrm{m}$, $t_0 = 0.9022\,\mathrm{s}$ and $\dot{\theta} = -5.9240\,\mathrm{rad/s}$; (b) $A = 0.6\,\mathrm{m}$, $t_0 = 0.8343\,\mathrm{s}$ and $\dot{\theta} = -6.1234\,\mathrm{rad/s}$; (c) $A = 0.7\,\mathrm{m}$, $t_0 = 0.9644\,\mathrm{s}$ and $\dot{\theta} = -8.9100\,\mathrm{rad/s}$; (d) $A = 0.75\,\mathrm{m}$, $t_0 = 0.98762\,\mathrm{s}$ and $\dot{\theta} = -9.3623\,\mathrm{rad/s}$) for the analytical solution of perioid-1 impact motion with parameters: $M = 1200\,\mathrm{kg}$, $m = 150\,\mathrm{kg}$, $J_M = 2500\,\mathrm{kgm^2}$, $C_1 = C_2 = 4\,\mathrm{kN\,s/m}$, $K_1 = 30\,\mathrm{kN/m}$, $K_2 = 40\,\mathrm{kN/m}$, $K_3 = 400\,\mathrm{N/m}$, $L = 0.6\,\mathrm{m}$, $a_1 = 0.5\,\mathrm{m}$, $a_2 = 0.3\,\mathrm{m}$, ground sinusoidal wavelength $B = 10\,\mathrm{m}$, vehicle's velocity $v = 10\,\mathrm{m/s}$, and impact restitution coefficients $\mu_1 = \mu_2 = 0.8$).

$A_{cr6} < A < A_{cr7}$, the period-2 motion has two cycles during N-periods with four impacts on the two walls, as demonstrated in Fig. 6(c) for $A = 0.47\,\mathrm{m}$. After the impact motion model switches, we can observe the motion possessing two continuous impacts on the one wall and one impact on the other wall, as shown in Fig. 6(d) for $A = 0.8\,\mathrm{m}$. In Fig. 7(a), the impact period-1 motion for $A = 0.4\,\mathrm{m}$ is simulated for comparison with the period-1 motion without damping. Furthermore, after the period-doubling bifurcation, the period-2 motion is illustrated in Fig. 7(b) for $A = 0.6\,\mathrm{m}$. In addition, another type of the period-1 motion for two impacts, respectively, on the two walls during a certain period is shown in Fig. 7(c) for $A = 0.7\,\mathrm{m}$. The period-doubling bifurcation gives a period-2 motion for such an impact model, as is plotted in Fig. 7(d) for $A = 0.75\,\mathrm{m}$.

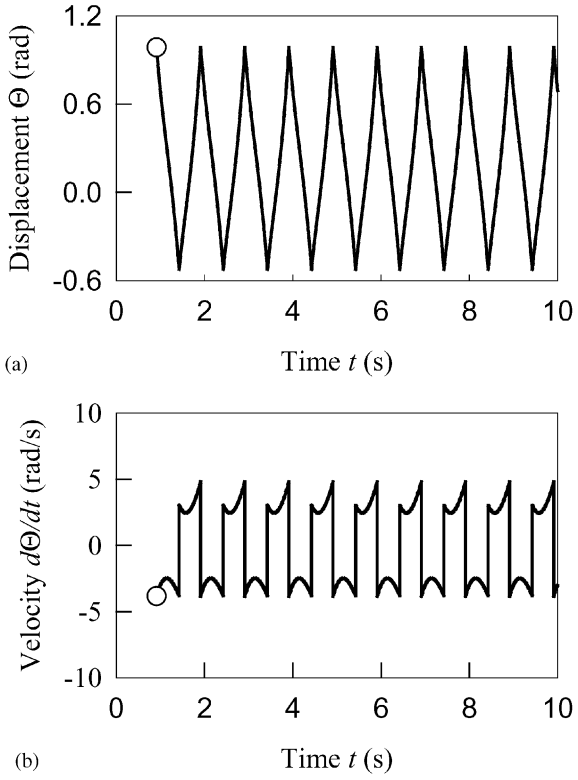

Fig. 8. The (a) relative displacement ($\Theta = \theta - \psi$) and (b) velocity responses ($C_3 = 0$, $A = 0.1$ m, and initial conditions: $t_0 = 0.9187$ s, $\theta = 0.9851$ rad, $\dot{\theta} = -4.2692$ rad/s) with parameters $M = 1200$ kg, $m = 150$ kg, $J_M = 2500$ kg m^2, $C_1 = C_2 = 4$ kN s/m, $K_1 = 30$ kN/m, $K_2 = 40$ kN/m, $K_3 = 400$ N/m, $L = 0.6$ m, $a_1 = 0.5$ m, $a_2 = 0.3$ m, ground sinusoidal wavelength $B = 10$ m, vehicle's velocity $v = 10$ m/s, and impact restitution coefficients $\mu_1 = \mu_2 = 0.8$.

For a better understanding of such periodic impact motions, the relative displacement and velocity responses of passengers are shown in Figs. 8–11 for $C_3 = 0$. In Fig. 8, the displacement response is almost symmetric and the time intervals from one wall to the other are almost equal. The discontinuity and asymmetry of the velocity response is very clearly illustrated. Increasing the ground amplitude, in Fig. 9, the asymmetry for displacement and velocity responses is observed. The velocities in the forwarding and returning motions are distinguishing. The forwarding motion of passengers is faster than the returning motion. With further increasing amplitude, such an asymmetric phenomenon becomes more predominant, as shown in Fig. 10. In Fig. 11, the period-1 motion with two impacts on the front wall (wall-1) and one impact on the back wall (wall-2) are illustrated. The analytical prediction of this passenger motion is not completed, and further investigations should be carried out.

5. Conclusion

The period-1 impact motion of passenger in vehicles traveling on rough terrain is predicted analytically and numerically through a linear model. The stability and bifurcation of such a period-1 impact motion are developed. In this mechanical model, the human body is considered as a massless

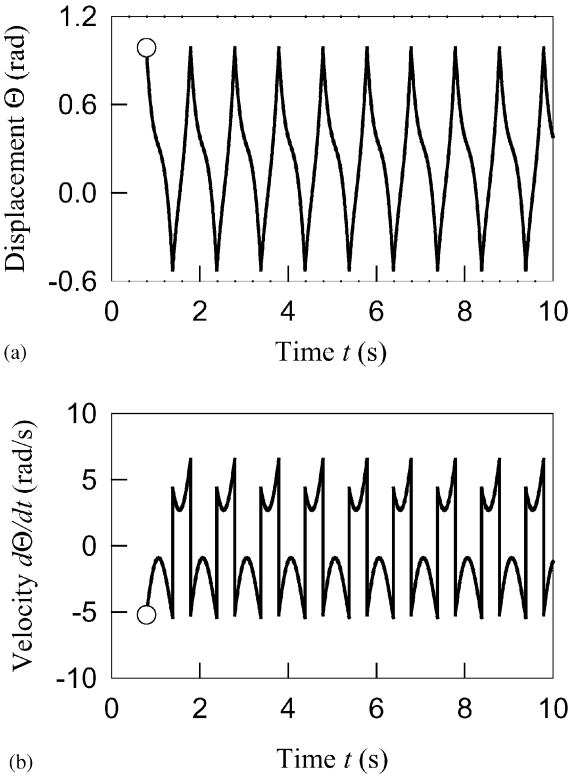

Fig. 9. The (a) relative displacement ($\Theta = \theta - \psi$) and (b) velocity responses ($C_3 = 0$, $A = 0.4$ m, and initial conditions: $t_0 = 0.7936$ s, $\theta = 0.9851$ rad, $\dot{\theta} = -5.2655$ rad/s) with parameters $M = 1200$ kg, $m = 150$ kg, $J_M = 2500$ kgm^2, $C_1 = C_2 = 4$ kN s/m, $K_1 = 30$ kN/m, $K_2 = 40$ kN/m, $K_3 = 400$ N/m, $L = 0.6$ m, $a_1 = 0.5$ m, $a_2 = 0.3$ m, ground sinusoidal wavelength $B = 10$ m, vehicle's velocity $v = 10$ m/s, and impact restitution coefficients $\mu_1 = \mu_2 = 0.8$.

bar with a lumped mass. Although the mechanical model used in this paper is an idealized one, the dynamic responses of the human body in vehicles traveling on rough terrain as analyzed here is useful for the rough evaluation of human body safety in traveling vehicles. In the future, a more realistic model should be developed for a better prediction of human body motion and safety.

Appendix A. Coefficients and eigenvalue analysis

In Eq. (14), the constants γ_1 and γ_2 are given by

$$\gamma_1 = -\frac{Mg(K_1 + K_2)}{4K_1K_2}, \quad \gamma_2 = \frac{Mg(K_2 - K_1)}{4K_1K_2b} \tag{A.1}$$

and the α_i and β_i $(i = 1, 2)$ are computed by

$$\begin{bmatrix} \alpha_1 \\ \alpha_2 \\ \beta_1 \\ \beta_2 \end{bmatrix} = \begin{bmatrix} n_1 & n_2 & n_3 & n_4 \\ -n_2 & n_1 & -n_4 & n_3 \\ n_3 & n_4 & n_5 & n_6 \\ -n_4 & n_3 & -n_6 & n_5 \end{bmatrix}^{-1} \begin{bmatrix} m_1 \\ m_2 \\ m_3 \\ m_4 \end{bmatrix}, \tag{A.2}$$

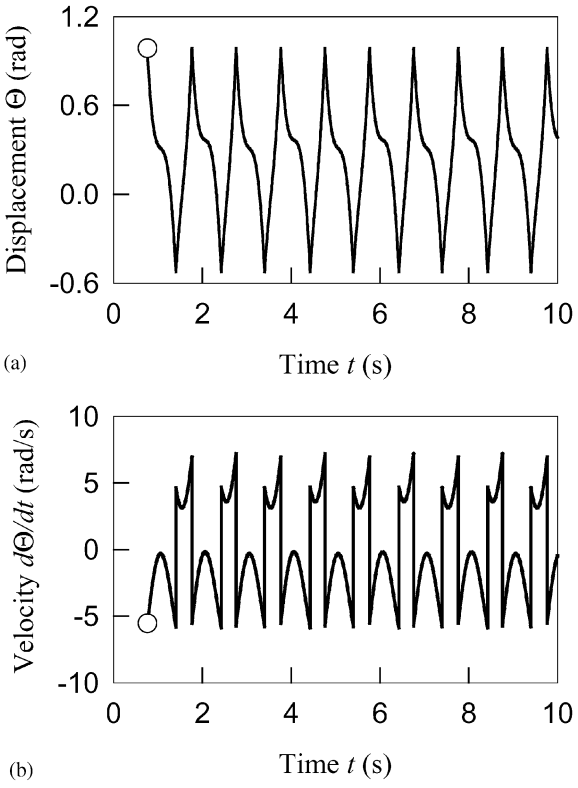

Fig. 10. The (a) relative displacement ($\Theta = \theta - \psi$) and (b) velocity responses ($C_3 = 0$, $A = 0.47$ m, and initial conditions: $t_0 = 0.7655$ s, $\theta = 0.9851$ rad, $\dot{\theta} = -5.4197$ rad/s) with parameters $M = 1200$ kg, $m = 150$ kg, $J_M = 2500$ kgm^2, $C_1 = C_2 = 4$ kN s/m, $K_1 = 30$ kN/m, $K_2 = 40$ kN/m, $K_3 = 400$ N/m, $L = 0.6$ m, $a_1 = 0.5$ m, $a_2 = 0.3$ m, ground sinusoidal wavelength $B = 10$ m, vehicle's velocity $v = 10$ m/s, and impact restitution coefficients $\mu_1 = \mu_2 = 0.8$.

where

$$n_1 = -\omega^2 M + (K_1 + K_2), \quad n_2 = -\omega(C_1 + C_2), \quad n_3 = (K_2 - K_1)b,$$
$$n_4 = -\omega(C_2 - C_1)b, \quad n_5 = -\omega^2 J_M + (K_1 + K_2)b^2, \quad n_6 = -\omega(C_1 + C_2)b^2, \tag{A.3}$$

$$m_1 = K_1 A + K_2 A\cos\phi + C_2 A\omega\sin\phi, \quad m_2 = C_1 A\omega - K_2 A\sin\phi + C_2 A\omega\cos\phi,$$
$$m_3 = -K_1 bA + K_2 bA\cos\phi + C_2 bA\omega\sin\phi, \quad m_4 = -C_1 bA\omega - K_2 bA\sin\phi + C_2 bA\omega\cos\phi. \tag{A.4}$$

The eigenvalues λ_i ($i = 1, 2, \ldots, 4$) are determined by

$$\left| -\left(\mathbf{M}^*\right)^{-1}\mathbf{A}^* - \lambda\mathbf{I} \right| = 0, \tag{A.5}$$

where $\mathbf{I}$ is a 4×4 identity matrix

$$\mathbf{M}^* = \begin{bmatrix} \mathbf{I} & \mathbf{0} \\ \mathbf{0} & \mathbf{m}^* \end{bmatrix}, \quad \mathbf{A}^* = \begin{bmatrix} \mathbf{0} & -\mathbf{I} \\ \mathbf{K}_1^* & \mathbf{C}_1^* \end{bmatrix}. \tag{A.6}$$

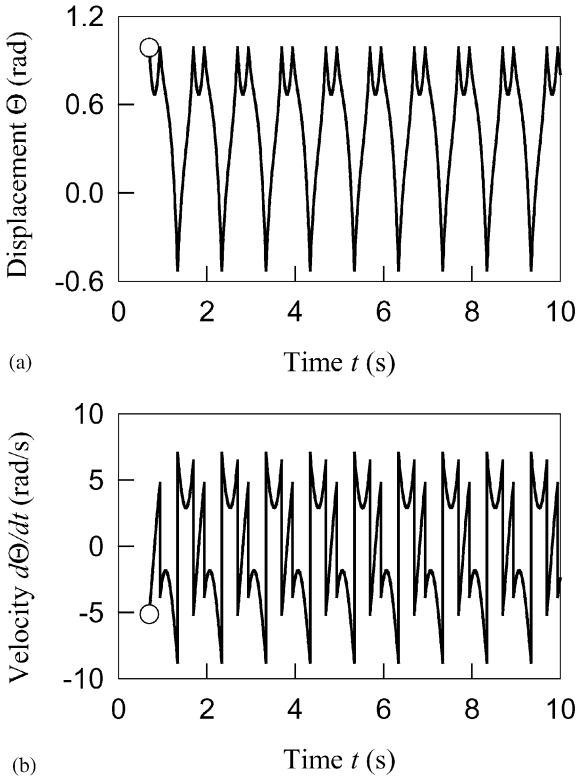

Fig. 11. The (a) relative displacement ($\Theta = \theta - \psi$) and (b) velocity responses ($C_3 = 0$, $A = 0.8$ m, and initial conditions: $t_0 = 0.7006$ s, $\theta = 0.9851$ rad, $\dot{\theta} = -7.2166$ rad/s) with parameters $M = 1200$ kg, $m = 150$ kg, $J_M = 2500$ kg m^2, $C_1 = C_2 = 4$ kN s/m, $K_1 = 30$ kN/m, $K_2 = 40$ kN/m, $K_3 = 400$ N/m, $L = 0.6$ m, $a_1 = 0.5$ m, $a_2 = 0.3$ m, ground sinusoidal wavelength $B = 10$ m, vehicle's velocity $v = 10$ m/s, and impact restitution coefficients $\mu_1 = \mu_2 = 0.8$.

Note that the 2×2 identity and zero matrices are denoted by $\mathbf{I}$ and $\mathbf{0}$, and

$$\mathbf{m}^* = \begin{bmatrix} M & 0 \\ 0 & J_M \end{bmatrix}, \quad \mathbf{C}_1^* = \begin{bmatrix} C_1 + C_2 & (C_2 - C_1)b \\ (C_2 - C_1)b & (C_1 + C_2)b^2 \end{bmatrix},$$
$$\mathbf{K}_1^* = \begin{bmatrix} K_1 + K_2 & (K_2 - K_1)b \\ (K_2 - K_1)b & (K_1 + K_2)b^2 \end{bmatrix}. \tag{A.7}$$

In Eq. (15), constants A_1^*, A_2^*, A_3^* are:

$$A_1^* = \frac{S_1\beta_1 + S_2\beta_2}{S_d}, A_2^* = \frac{S_1\beta_2 - S_2\beta_1}{S_d}, \text{ and } A_3^* = \frac{K_3\gamma_2}{K_3 - mgL}; \tag{A.8}$$

where

$$S_1 = C_3^2\omega^2 + K_3(K_3 - mgL - mL^2\omega^2), \quad S_2 = K_3C_3\omega - C_3\omega(K_3 - mgL - mL^2\omega^2),$$
$$S_d = (K_3 - mgL - mL^2\omega^2)^2 + C_3^2\omega^2. \tag{A.9}$$

The eigenvalues are

$$\lambda_{1,2} = \frac{-C_3 \pm \sqrt{C_3^2 - 4mL^2(K_3 - mgL)}}{2mL^2}. \tag{A.10}$$

In Eq. (34), the matrices components are computed by

$$\begin{bmatrix} \dfrac{\partial g_1}{\partial t_{i+1}} & 0 & 0 & 0 \\ 0 & \dfrac{\partial g_1}{\partial t_{i+1}} & 0 & 0 \\ \dfrac{\partial g_2}{\partial t_{i+1}} & 0 & -1 & 0 \\ 0 & \dfrac{\partial g_2}{\partial t_{i+1}} & 0 & -1 \end{bmatrix} \begin{pmatrix} \dfrac{\partial t_{i+1}}{\partial t_i} \\ \dfrac{\partial t_{i+1}}{\partial \dot{\Theta}_i} \\ \dfrac{\partial \dot{\Theta}_{i+1}}{\partial t_i} \\ \dfrac{\partial \dot{\Theta}_{i+1}}{\partial \dot{\Theta}_i} \end{pmatrix} + \begin{pmatrix} \dfrac{\partial g_1}{\partial t_i} \\ \dfrac{\partial g_1}{\partial \dot{\Theta}_i} \\ \dfrac{\partial g_2}{\partial t_i} \\ \dfrac{\partial g_2}{\partial \dot{\Theta}_i} \end{pmatrix} = 0 \tag{A.11}$$

and

$$\begin{bmatrix} \dfrac{\partial g_3}{\partial t_{i+2}} & 0 & 0 & 0 \\ 0 & \dfrac{\partial g_3}{\partial t_{i+2}} & 0 & 0 \\ \dfrac{\partial g_2}{\partial t_{i+2}} & 0 & -1 & 0 \\ 0 & \dfrac{\partial g_2}{\partial t_{i+2}} & 0 & -1 \end{bmatrix} \begin{pmatrix} \dfrac{\partial t_{i+2}}{\partial t_{i+1}} \\ \dfrac{\partial t_{i+2}}{\partial \dot{\Theta}_{i+1}} \\ \dfrac{\partial \dot{\Theta}_{i+2}}{\partial t_{i+1}} \\ \dfrac{\partial \dot{\Theta}_{i+2}}{\partial \dot{\Theta}_{i+1}} \end{pmatrix} + \begin{pmatrix} \dfrac{\partial g_3}{\partial t_{i+1}} \\ \dfrac{\partial g_3}{\partial \dot{\Theta}^+_{i+1}} \\ \dfrac{\partial g_2}{\partial t_{i+1}} \\ \dfrac{\partial g_2}{\partial \dot{\Theta}^+_{i+1}} \end{pmatrix} = 0, \tag{A.12}$$

where

$$\begin{aligned} \Theta_{r1} &= g_1(t_{i+1}, t_i, \dot{\Theta}_i) = A_1 \sin \omega t_{i+1} + A_2 \cos \omega t_{i+1} + A_3 + A_4^{(i)} e^{\lambda_1 (t_{i+1} - t_i)} + A_5^{(i)} e^{\lambda_2 (t_{i+1} - t_i)}, \\ \dot{\Theta}_{i+1} &= g_2(t_{i+1}, t_i, \dot{\Theta}_i) = -\mu_2 (A_1 \omega \sin \omega t_{i+1} - A_2 \omega \cos \omega t_{i+1} + A_4^{(i)} \lambda_1 e^{\lambda_1 (t_{i+1} - t_i)} + A_5^{(i)} \lambda_2 e^{\lambda_2 (t_{i+1} - t_i)}), \end{aligned} \tag{A.13}$$

$$\begin{aligned} \Theta_{r2} &= g_3(t_{i+2}, t_{i+1}, \dot{\Theta}_{i+1}) \\ &= A_1 \sin \omega t_{i+2} + A_2 \cos \omega t_{i+2} + A_3 + A_4^{(i+1)} e^{\lambda_1 (t_{i+2} - t_{i+1})} + A_5^{(i+1)} e^{\lambda_2 (t_{i+2} - t_{i+1})}, \\ \dot{\Theta}_{i+2} &= g_4(t_{i+2}, t_{i+1}, \dot{\Theta}_{i+1}) \\ &= -\mu_1 (A_1 \omega \sin \omega t_{i+2} - A_2 \omega \cos \omega t_{i+2} + A_4^{(i+1)} \lambda_1 e^{\lambda_1 (t_{i+2} - t_{i+1})} + A_5^{(i+1)} \lambda_2 e^{\lambda_2 (t_{i+2} - t_{i+1})}). \end{aligned} \tag{A.14}$$

References

[1] R.R. Coermann, The mechanical impedance of the human body in sitting and standing position at low frequencies, *Human Factor* 4 (1962) 227–253.

[2] A. Wisner, A. Donnadiu, A. Berthoz, A biomechanical model of man for the study of vehicle seat and suspension, *International Journal of Production Research* 3 (4) (1964) 285–315.
[3] C.W. Suggs, C.F. Abrams, L.F. Stikeleather, Application of a damped spring-mass human vibration simulation in vibration testing of vehicle seats, *Ergonomics* 12 (1) (1969) 79–90.
[4] M.J. Griffin, E.M. Whithan, K.C. Paesons, Vibration and comfort I—translational seat vibration, *Ergonomics* 5 (7) (1982) 603–630.
[5] O.B. Ahmed, J.F. Goupillon, Predicting the ride vibration of an agricultural tractor, *Journal of Terramechanics* 34 (1997) 1–11.
[6] V.K. Tewari, N. Prasad, Three-DOF modeling of tractor seat-operator system, *Journal of Terramechanics* 36 (1999) 207–219.
[7] K. Yu, A.C.J. Luo, Y. He, Stability and vibration of a nonlinear vehicle and passenger system, *Proceedings of the Institution of Mechanical Engineers, Part K: Journal of Multibody Dynamics* 216 (2002) 109–116.
[8] F. Hendricks, Bounce and chaotic motion in impact print hammers, *IBM Journal* 27 (1983) 273–280.
[9] P.C. Tung, S.W. Shaw, The dynamics of an impact print hammer, *Journal of Vibration Acoustics Stress Reliability Design* 110 (1988) 193–200.
[10] M. Sharif-Bakhtiar, S.W. Shaw, The dynamic response of a centrifugal pendulum absorber with motion limiting stops, *Journal of Sound and Vibration* 126 (1988) 221–235.
[11] K. Karagiannis, F. Pfeiffer, Theoretical and experimental investigation of gear rattling, *Nonlinear Dynamics* 2 (1991) 367–387.
[12] A. Kahraman, R. Singh, Nonlinear dynamics of a spur gear pair, *Journal of Sound and Vibration* 142 (1990) 49–75.
[13] S.F. Masri, T.D. Caughey, On the stability of the impact damper, *American Society of Mechanical Engineers, Journal of Applied Mechanics* 33 (1966) 586–592.
[14] C.N. Bapat, N. Popplewell, K. Mclachlan, Stable periodic motion of an impact pair, *Journal of Sound and Vibration* 87 (1983) 19–40.
[15] C.N. Bapat, S. Sankar, Single unit impact damper in free and forced vibrations, *Journal of Sound and Vibration* 99 (1985) 85–94.
[16] R.P.S. Han, A.C.J. Luo, W. Deng, Chaotic motion of a horizontal impact pair, *Journal of Sound and Vibration* 181 (1995) 231–250.
[17] A.C.J. Luo, An unsymmetrical motion in a horizontal impact oscillator, *American Society of Mechanical Engineers, Journal of Vibration and Acoustics* 124 (2002) 420–426.